



Contents lists available at ScienceDirect

Optik

journal homepage: [www.elsevier.com/locate/ijleo](http://www.elsevier.com/locate/ijleo)

Original research article

# Lily (*Iris Persica*) pigments as new sensitizer and TiO<sub>2</sub> nanofibers as photoanode electrode in dye sensitized solar cells

Shadman Mansouri<sup>a</sup>, Mohammad Hossein Abbaspour-Fard<sup>a,\*</sup>, Azadeh Meshkini<sup>b</sup><sup>a</sup> Department of Biosystems Engineering, Faculty of Agriculture, Ferdowsi University of Mashhad, P.O. Box 91775-1163, Mashhad, Iran<sup>b</sup> Department of Chemistry, Faculty of Science, Ferdowsi University of Mashhad, P.O. Box 91775-1436, Mashhad, Iran

## ARTICLE INFO

## Keywords:

Dye sensitized solar cell (DSSC)

Wild lily dyes

TiO<sub>2</sub> nanofibers

Electrospinning

## ABSTRACT

In this study, lily (*Iris Persica*) dyes as sensitizer were examined by UV-vis and FTIR analyses. Corresponding results showed that lily pigments effectively absorb incident light. This was mainly due to the presence of functional groups such as C=O and O-H in the pigment structure appeared on the FTIR analysis. This shows the appropriateness of lily pigment as sensitizer. On the other hand, anatase TiO<sub>2</sub> nanofibers with different diameters were synthesized by Electrospinning method, using Titanium isopropoxide (TIPP) and polyvinylpyrrolidone (PVP) solution. The Electrospinning feed rate was altered from 0.1 to 0.5 mL/h to control the diameter of the TiO<sub>2</sub> nanofibers. Other effective parameters including voltage, needle tip distance to collector and speed of collector were 25 kV, 15 cm and 500 rpm, respectively and were kept constant during synthesizing of nanofibers. The Synthesized nanofibers were analyzed and characterized by means of SEM, FESEM, XRD and TEM techniques. The FESEM and XRD analyses indicated that the nanofiber's diameter and crystallinity increase with increase in feed rate. The fabricated DSSC with 430 nm TiO<sub>2</sub> nanofibers (obtained from flow rate of 0.3 mL/h) provided 1.72 % energy conversion efficiency ( $\eta$ ), 50.78 % conversion efficiency of photon to electron (IPCE), short-circuit current density ( $J_{sc}$ ) of 2.716 mA/cm<sup>2</sup> and open circuit voltage ( $V_{oc}$ ) of 0.738 V. The efficiency of the developed DSSCs, in comparison with the previously fabricated similar cells, were found higher, due to more effective absorption of light by the dyes and adsorption of pigment by nanofibers.

## 1. Introduction

Dye sensitized solar cells (DSSCs) are cost effective type of solar cells with wonderful advantages [1,2] that makes them as top substitute to conventional solar cells. To commercialize the DSSCs, investigations are on the go [e.g. 3]. The dye sensitized solar cells were primarily introduced by Grätzel and O'Regan in 1990 [2] followed by 7 % efficiency development in 1991 [4,5]. Since then efficiency was gradually improved to 11 % [6]. Mathew et al. enhanced power conversion efficiency of DSSC cells up to 13 % [7]. Efficiencies of natural dyes were improved to a maximum of 14.7 % [8]. However, to overtake silicon solar cells, efficiency should be greater than 20 % [9]. The structure of DSSC solar cells comprises three main components (Fig. 1) [4,7,10].

The DSSC working cycle can be found elsewhere [7,11]. The performance of DSSCs is affected by photoanode [12] and dye sensitizers. In the meantime, researchers found natural dyes interesting [3,13]. In comparison with synthetic or artificial dyes, natural

\* Corresponding author at: Department of Biosystems Engineering, Faculty of Agriculture, Ferdowsi University of Mashhad, University campus, Azadi Square, P.O. Box 91775-1163, Mashhad, Iran.

E-mail addresses: [sh\\_ma591@mail.um.ac.ir](mailto:sh_ma591@mail.um.ac.ir) (S. Mansouri), [abaspur@um.ac.ir](mailto:abaspur@um.ac.ir) (M.H. Abbaspour-Fard), [a.meshkini@um.ac.ir](mailto:a.meshkini@um.ac.ir) (A. Meshkini).

<https://doi.org/10.1016/j.ijleo.2019.163710>

Received 28 July 2019; Received in revised form 21 October 2019; Accepted 5 November 2019

0030-4026/ © 2019 Elsevier GmbH. All rights reserved.

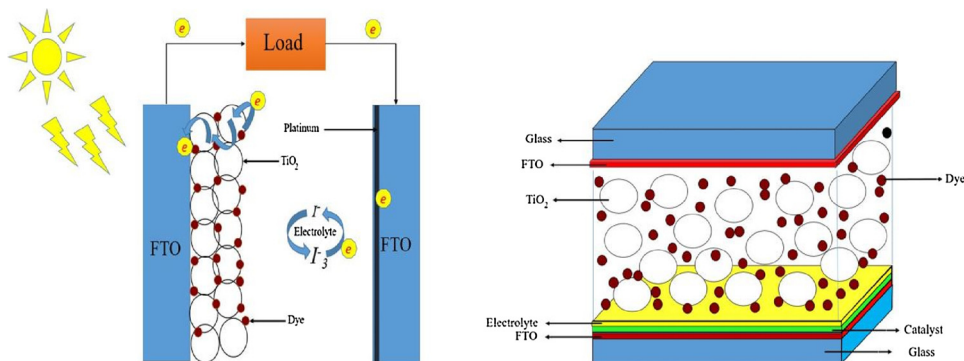


Fig. 1. DSSC structure and principle.

dyes are eco-friendly, cheap, easy to extract and abundantly available [11], but the cells produced from these dyes have conversion efficiency as low as 5 % [14]. Nevertheless, appropriate dyes would have the advantages of both natural and artificial dyes, while exempt from their drawbacks. This challenge can be overcome by appropriate selection of natural dyes [15] for an optimized electron injection.

Nanoparticles have numerous inter-particle boundaries, which slow down electron velocity and increase electron recombination or electron trapping. To resolve this problem, it is necessary to examine other nanostructures such as nanofibers [16].

Song et al. and Mali et al. employed  $\text{TiO}_2$  nanofibers and a chemical sensitizer to fabricate DSSCs [17,18]. They concluded that employing  $\text{TiO}_2$  nanofibers instead of  $\text{TiO}_2$  nanoparticles improves the photovoltaic properties of DSSCs.

In the current study, the  $\text{TiO}_2$  nanofibers and the natural pigments were combined in photoanode for the first time. Wild Lily flowers were used because their dyes contain anthocyanin which is well bonded to  $\text{TiO}_2$  nanostructure and absorbs solar spectrum in a wider UV-vis region. Moreover, electrospun  $\text{TiO}_2$  nanofibers adsorb dyes in a larger surface and would make individual pathways for electrons, hence preventing the recombination problem and speed up the electron cycle in the fabricated DSSCs.

## 2. Material and methods

### 2.1. Chemicals and materials

Titanium (IV isopropoxide ( $\text{Ti}(\text{OiPr})_4$ ) and polyvinylpyrrolidone (PVP) (PVP K90, MW = 1.300.000) were purchased from Sigma-Aldrich. Magnesium powder, acetic acid glacial (99.8 % purity), acetic anhydride, iodine ( $\text{I}_2$ ), chromic oxide ( $\text{CrO}_3$ ) and absolute Ethanol (99.99 % purity) were ordered from Merck.

### 2.2. Electrospinning

In the first step, 2 mL  $\text{Ti}(\text{OiPr})_4$  was mixed with 2 mL ethanol and 2 mL acetic acid. In the second step, 0.6 g of PVP was mixed with 6 mL of ethanol. Both solutions were then stirred for about 15 min. Then the first solution was added to the polymer solution drop by drop. After one hour of stirring, the mixed solution was heated to 50 °C until a viscous solution was resulted. As TIPP reacts with air moisture, ethanol and acetic acid were dried to remove the trace of water [19,20]. All materials need to be stored in a vacuum desiccator.

The prepared solution was loaded into a syringe pump, equipped with a 21-gage stainless steel needle. The electrospinning runs were performed with three different flow rates, while the other factors were kept constant. The morphology and diameter of the  $\text{TiO}_2$  nanofibers were analyzed by SEM (Leo 1450 VP, Germany) and FESEM (MIRA3 TE SCAN, Czech Republic). Morphological and structural analyses were investigated by TEM (Leo 912 AB, Germany). FTIR was used to find the functional groups of the  $\text{TiO}_2$  nanostructures.

### 2.3. Dye extraction procedure

Lily flowers were harvested from Kurdistan Mountains in Iran. Fresh flowers were carefully washed with deionized water and dried in natural air condition, away from direct sunlight. The dyes extraction done according to others [21,22].

### 2.4. DSSC fabrication

FTO (glass sheet with 10  $\Omega/\text{cm}^2$ ) was cleaned to remove residual organic contaminants for better efficiency [23]. The FTO was coated by calcined electrospun  $\text{TiO}_2$  nanofibers paste and heated at about 500 °C. The prepared electrode was immersed in the solution of ethanol and the extracted dyes with ratio of 1:1 for about 24 h. The adsorbed dyes were measured by UV-vis spectrophotometer. A similar procedure was used for the preparation of the other electrode (Pt/FTO). I-V test, IPCE and UV-vis analyses

**Table 1**Structural properties and Summary of Photovoltaic performance parameters of the DSSCs (effective area = 0.5 cm<sup>2</sup>).

No.	Sample <sup>a</sup>	Dye adsorbed (μmol/cm <sup>2</sup> )	Thickness of TiO <sub>2</sub> films (μm)	V <sub>oc</sub> (V)	J <sub>sc</sub> (mA/cm <sup>2</sup> )	FF (%)	η (%)	IPCE (%)
1	P25	69	11.00	0.331	2.122	84	0.590	36.67
2	210 nm	76	15.20	0.511	1.710	81	0.708	27.92
3	425 nm	93	14.75	0.738	2.716	86	1.720	50.78
4	631 nm	84	13.40	0.524	3.095	76	1.230	42.70

<sup>a</sup> Numbers refer to the diameter of nanoparticle and/or nanofibers.

were carried out to characterize the fabricated DSSCs.

### 3. Results and discussion

**Table 1** shows the structural properties and photovoltaic performance of the DSSCs fabricated with three different diameters of nanofibers.

As seen in **Table 1** the DSSC sample consists of nanofibers with average diameter of 425 nm provided a higher conversion efficiency than the other samples.

**Fig. 2** illustrates the SEM images of the electrospun TiO<sub>2</sub>/PVP nanofibers. The average diameter of the produced nanofibers for the flow rates of 0.1, 0.3 and 0.5 mL/h were 374, 569 and 710 nm, respectively. As PVP polymer removed from the composite nanofibers by heating at 510 °C in air, the diameter of the remaining pure TiO<sub>2</sub> nanofibers reduced to 210, 425, and 631 nm for the flow rates of 0.1, 0.3 and 0.5 ml/h, respectively. Decreasing the thickness was mainly due to the evaporation of PVP [24].

**Fig. 2** also shows the FESEM analyze of the electrospun TiO<sub>2</sub>/PVP composite nanofibers. In the FESEM images, it is clear that the produced nanofibers are straight, smooth and have mesoporous structure. **Fig. 3B** shows that they are actually composed of nanoparticles, with rod like arrangement.

Crystal phase of the mesoporous nanofibers was determined by X-ray diffraction (XRD) using CuKα radiation (λ = 1.54 Å) at 40 kV and 30 mA comprises a size step of 0.040° and time step of 1 s (EXPLORER, GNR, Italy). **Fig. 3A** shows the XRD record for the calcinated electrospun TiO<sub>2</sub> nanofibers, illustrating the formation of pure anatase phase after calcination at 510°C in airflow for two hours. Pulverizing process in electrospinning took place when the concentration of PVP was lower than the usual mode [25].

Transforming from anatase to rutile phase occurred when the temperature of calcination increased to above 600°C [26]. The anatase phase of nanofibers causes higher electron transport ability in DSSCs and hence enhances their performance [27]. For this reason, the anatase phase is preferred and the calcination was carried out below 600 °C.

The peaks at 25.5°, 38.8°, 48.08°, 54.94°, 62.79°, 69.31°, 70.11° and 75.58° are correspond to the planes of (101), (004), (200), (105), (211), (204), (116), (220) and (215) respectively are related to the anatase phase of TiO<sub>2</sub> nanofibers (**Fig. 3A**). It is also clear from the results of XRD analysis that the crystalline structure improves with increasing injection rate, which results in increasing the thickness of nanofibers.

**Fig. 3B** also shows the TEM image of the synthesized nanofibers. As image reveals, the fibers are uniform and were synthesized with appropriate lengths. A single-strand fiber is also shown in this figure to illustrate the structure of fibers clearly. The structure of fibers are clustered in crystals that are arranged in a cylindrical structure. In addition, TEM images represent a periodic atomic arrangement to form an atomic network with good crystalline structure of nanofibers.

The surface area by Electron Diffraction pattern (SAED) for the synthesized TiO<sub>2</sub> nanofibers is shown in **Fig. 3B**. This template can examine the accuracy of XRD analysis. The formation of a dotted-line ring pattern represents poly-crystalline nature of TiO<sub>2</sub> nanofibers. The template clearly shows the presence of crystalline anatase phase and lack of rutile phase in the nanofibers structure [26].

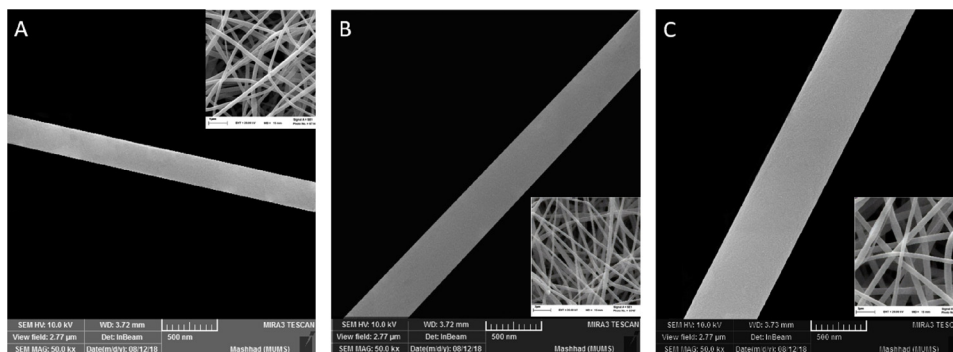


**Fig. 2.** Scanning Electron Microscopic (SEM) and Field Emission Scanning Electron Microscopic (FESEM) images of the synthesized anatase TiO<sub>2</sub> nanofibers deposited by different feed rates: (A) 0.1 mL/h (B) 0.3 mL/h, and (C) 0.5 mL/h.

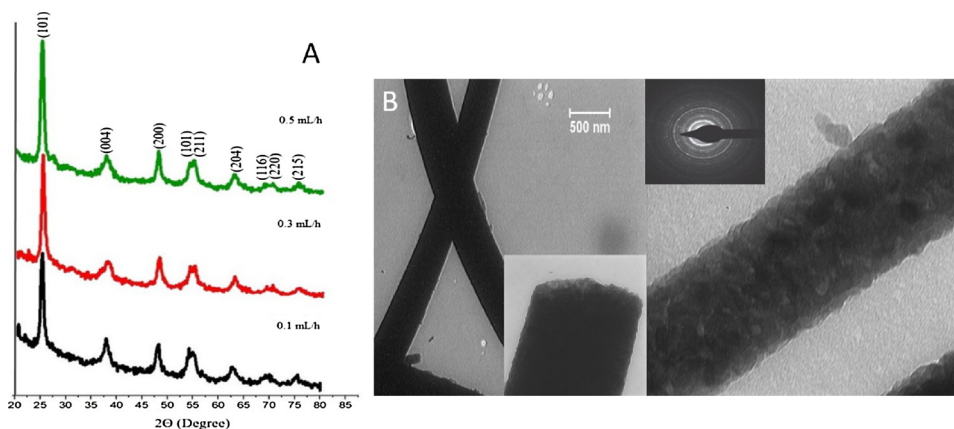


Fig. 3. A. XRD records of the calcinated electrospun TiO<sub>2</sub> nanofibers with different flow rate. B) TEM image of the synthesized nanofibers and Selected Area Electron Diffraction pattern (SAED) of the TiO<sub>2</sub> nanofibers.

Chemical absorption of pigments on the surface of TiO<sub>2</sub> nanostructures occurred due to the presence of hydroxyl (–OH), esters and carbonyl groups (C=O) in plant pigments [28,29]. Pure TiO<sub>2</sub> nanofibers show two absorption bands in the 2360 cm<sup>-1</sup> and 724 cm<sup>-1</sup> (Fig. 4). FTIR spectrum of the pigments shows a broadband appeared within 2800–3500 cm<sup>-1</sup> representing H-bonding through hydroxyl (–OH) of the anthocyanin structure. This band is widely observed in the spectrum of nanofibers containing pigments. Moreover, a peak at 1600 cm<sup>-1</sup> stands for carbonyl group in the anthocyanin structure, which is also observed in the spectrum of the pigmented nanofibers, as an evidence to prove that pigments are bonded to the surface of nanofibers. In addition, the bands appeared in the FTIR region from 2800–3500 cm<sup>-1</sup> represent C–O functional group [30].

Fig. 5A shows the absorption spectra of the lily pigment, marking pigment adsorption on nanoparticles and the TiO<sub>2</sub> nanofibers in the photoanode. Top absorbance for lily flower occurs where lambda max is shown within a range of wavelengths from 470–670 nm. This absorption peak at 470–670 nm is clear in the absorption diagram for all samples. The strong absorption in this range indicates the excitement band of lily dyes and corresponds to the results of IPCE data.

The amount of pigments adsorbed on photoanodes was also studied. The P25 electrode adsorbed 76 mg/cm<sup>2</sup> pigment. While, the TiO<sub>2</sub> nanofibers photoanodes with injection rates of 0.1, 0.3 and 0.5 mL/h, showed 87, 108 and 79 mg/cm<sup>2</sup> adsorbed pigment, respectively. The photoanode prepared by the TiO<sub>2</sub> nanofibers, provided from 0.3 mL/h flow rate showed more pigment adsorption than the others, and eventually improved the light absorption.

The photon-to-electron conversion efficiency (IPCE) of the DSSCs are shown in Fig. 5B. The Lily dyes sensitized solar cells exhibit maximum absorbance of about 580–690 nm for all TiO<sub>2</sub> nanostructures due to the effective adsorption of pigments. According to these results, the maximum IPCE observes for the nanofibers with average diameter of 425 nm. Clearly, IPCE is affected by incident

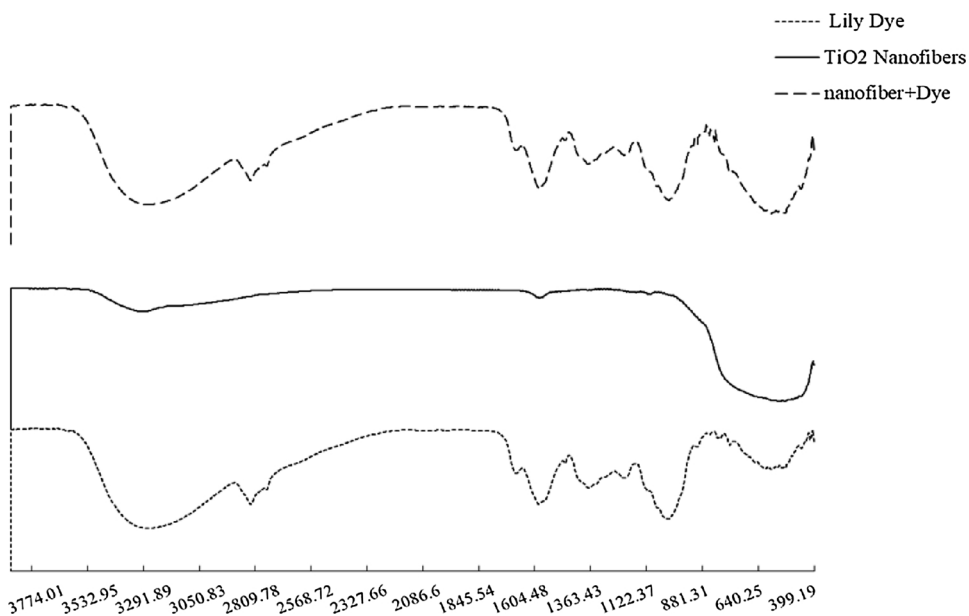


Fig. 4. FTIR spectrum of lily dye TiO<sub>2</sub> nanofibers and photoanode made with lily dyes and nanofibers.

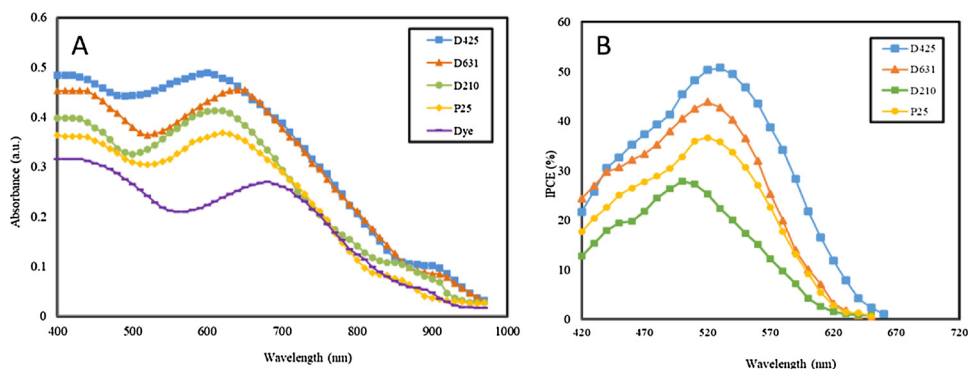


Fig. 5. A. Absorption spectra of the lily pigment, the pigment adsorbed by the nanoparticles (25 nm) and the TiO<sub>2</sub> nanofibers (210, 425 and 631 nm) in photoanode. B) The IPCE spectrum associated with the lily of the lime pigments absorbed on nanoparticles and TiO<sub>2</sub> nanofibers.

light or light intensity [31]. The maximum photon to electron efficiency for the cells made of P25 nanoparticles, nanofibers with diameter of 210, 425 and 631 nm, were 36.67, 27.92, 50.78 and 42.7%, respectively.

Fig. 6 shows the I–V diagram of the solar cells. The photovoltaic characteristics of the cells are also given in Table 2. These results show that the cell fabricated from nanofibers with 425 nm diameter has the highest energy conversion efficiency (1.72 %). This improvement was higher in efficiency than the other characteristics of nanofibers and nanoparticle cells. This also confirms the result of the IPCE. In fact, it is concluded that the nanofibers with diameter of 425 nm has the greatest pigment adsorption on their surface and the highest light absorption, and eventually the highest photon-to-electron conversion value.

The  $V_{OC}$  in the solar cells with electrode fabricated by nanofibers is more than that of comprising nanoparticles. Except from "D210", the  $J_{SC}$  of the cells made of nanofibers is higher than the cells fabricated by nanoparticles, this is mainly due to the resistance of  $R_{CT}$  in the nanoparticles. In other words, the higher cell resistance, the slower electron transfer in the electrolyte, which reduces efficiency of the cell. This interpretation was also verified for the differences  $V_{OC}$  [32].

The internal resistance and electron transfer properties were evaluated in the DSSCs sensitized with natural pigments, by EIS analysis. All EIS results are performed in dark conditions. The EIS fitted results and their data analysis are summarized in Fig. 7A and Table 2, respectively. Generally, the EIS of solar cells are three semicircular graphs that appear from high frequency to low frequency in Fig. 7A. These semicircles belong to charge-transfer resistance ( $R_1$ ), ( $R_2$ ) and  $R_3$ . The semicircles in the high frequency region of 20–100 Hz are related to ( $R_1$ ) and capacitor ( $C_{PE1}$ ). The semicircles in the intermediate range of frequencies (1–10 kHz) are due to ( $R_2$ . Charge transfer resistance and electron recombination ( $R_1$ ) and the chemical capacity ( $C_{PE1}$ ) at Dye / TiO<sub>2</sub> is related to the electron lifetime of the TiO<sub>2</sub> [17]. The high frequency (greater than 100 MHz) can be related to the general resistance ( $R_3$ ).

The charge transfer resistance ( $R_1$ ) is 25.30, 26.09, 29.45 and 24.44  $\Omega$ , charge transfer of ( $R_2$ ) is 158.25, 173.00, 198.30 and 162.10  $\Omega$ , respectively which are associated with the DSSCs (made of lily dye) of P25 nanoparticles and 210, 425 and 631 nm nanofibers, As shown in Table 2, the  $R_1$  and  $R_2$  are different for the cells with different pigments, as pigment molecules are bonded to

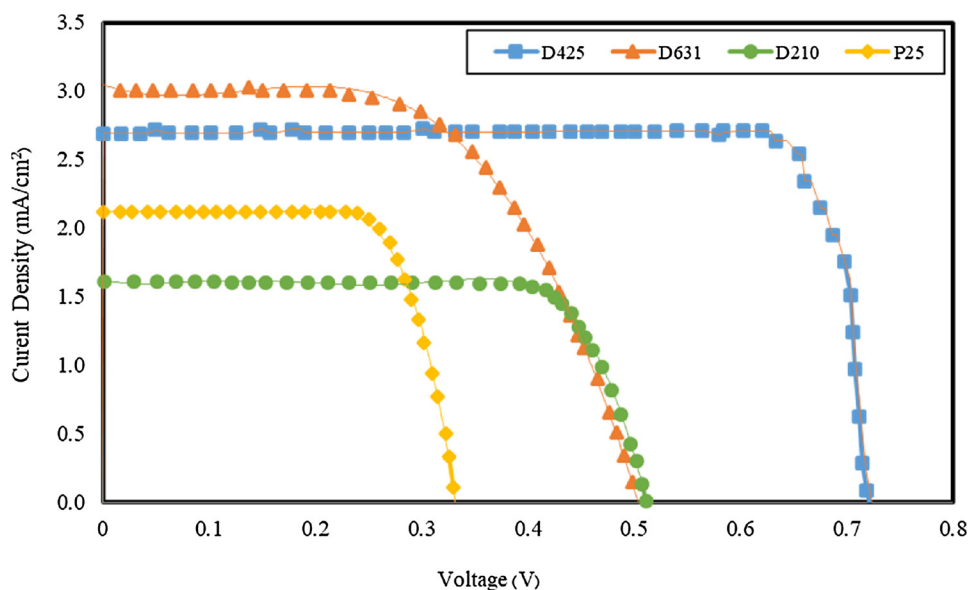
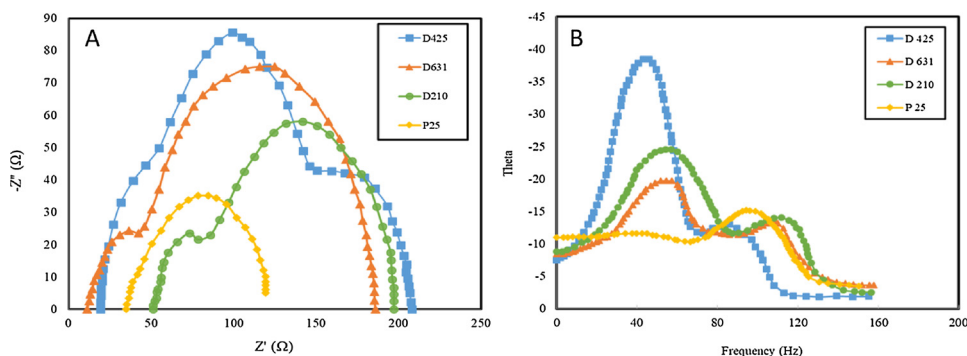


Fig. 6. The I–V diagram of the DSSCs sensitized with nanoparticles diameter of 25 nm and nanofibers of 210, 425 and 631 nm thickness.

**Table 2**

Impedance parameters of the DSSCs made of nanoparticles (P25) and the cells made of different nanofibers.

Cell type	Efficiency (%)	R <sub>1</sub> Pt / electrolyte	R <sub>2</sub> Electrolyte / Dye / TiO <sub>2</sub>	R <sub>s</sub>
P 25	0.59	25.30	158.25	83.0
210 nm	0.71	26.09	173.00	76.0
425 nm	1.72	29.45	198.30	54.0
631 nm	1.23	24.34	162.10	71.5



**Fig. 7.** A) Electrochemical impedance spectra of the DSSCs made of TiO<sub>2</sub> nanoparticles (P25), and TiO<sub>2</sub> nanofibers with different diameters. B) Bode phase plots of TiO<sub>2</sub> nanofibers. The X-axis is frequency (Hz) and Y-axis represented theta phase values.

titanium As reported by others [16]. Smaller R<sub>1</sub> and further R<sub>2</sub> increases TiO<sub>2</sub> / electrolyte resistance, which affect the suppressing electron recombination. These results are effective in very soft charge transfer and photoanode charge transfer efficiency of the cells made of nanofibers [17]. Therefore, the solar cell comprises of 425 nm nanofibers has the lowest electron recombination and hence the highest efficiency that matches with the results of I–V presented in Fig. 6.

Fig. 7B depicts the Bode phase diagrams of the solar cells sensitized with lily flower in frequency range of 0.1–1000 Hz, which is related to the effective lifetime of electrons on TiO<sub>2</sub> photoanode. The peak of the frequencies marked in each graph is inversely proportional to the lifetime of electrons [21,22]. The peak properties are transmitted to the low frequency from mid frequency based on the nanofibers provided from 0.1 to 0.3 flow rate, which is compared to P25 photoanode. 76.08 Hz, 13.58 Hz, 11.17 Hz, 18.69 Hz, and for P25, 210 nm, 425 nm and 631 nm are shown respectively. It should be noted that in the transmission of high frequency to low frequency, a fast transfer is shown as the electron lifetime ( $\tau_e$ ) is calculated from the following equation [33]:

$$\tau_e = 1/2\pi f_{\min}$$

where  $f_{\max}$  is the top frequency within frequency range. The lifetime of the electron for the cell provided from flow rate of 0.1 mL/h to 0.5 mL/h is 5.68–14.26 ms, respectively. The highest lifetime of electron was observed as 12–14.26 ms for the cell of using nanofibers of 425 nm, integrated from latest results where the 425 nm sample shows the lowest charge recombination and the highest electron lifetime. Hence, the results of bode phase diagram correspond to the I–V results.

#### 4. Conclusion

The DSSC fabricated and sensitized with TiO<sub>2</sub> nanoparticles could not exhibit desirable results, mainly due to the interfacial boundary between their layers and also electron recombination. The performance of the DSSCs sensitized with large and thick nanofibers (samples with average diameter of 631 nm) was also not good enough. This was mainly because of either low pigment adsorption or low light absorption. On the other hand, the small diameter nanofibers (210 nm) could not efficiently positively affect the performance of the DSSC, mostly because of reduced porosity or pigment adsorption. The best performance was achieved for the DSSC sensitized with 425 nm diameter nanofibers. Further investigations are required to optimize the selection of nanofibers for the best DSSC performance. In general, lily pigment due to its proper absorption on nanostructure and proper absorption of light is a good candidate as natural pigment. The reason for lower efficiency and higher recombination of electron in natural pigments compare to Synthetic pigments can be attributed to the poor bonding and high resistance of the former. Also the presence of COOH functional group and optimization of natural pigments is necessary to improve the efficiency of DSSCs.

#### Declaration of Competing Interest

The authors declare that they have no known competing financial interests or personal relationships that could have appeared to influence the work reported in this paper.

The authors declare the following financial interests/personal relationships which may be considered as potential competing

interests.

## Acknowledgements

The authors acknowledge financial supports received from Research deputy, Ferdowsi University of Mashhad. We also thank Ms. Yeganeh Naderi for technical support.

## References

- [1] W. Maiaugree, S. Lowpa, M. Towannang, P. Rutphonsan, A. Tangtrakarn, S. Pimanpang, P. Maiaugree, N. Ratchapolthavisin, W. Sang-Aroon, W. Jarernboon, A dye sensitized solar cell using natural counter electrode and natural dye derived from mangosteen peel waste, *Sci. Rep.* 5 (2015) 15230.
- [2] Y. Hao, W. Yang, L. Zhang, R. Jiang, E. Mijangos, Y. Saygili, L. Hammarström, A. Hagfeldt, G. Boschloo, A small electron donor in cobalt complex electrolyte significantly improves efficiency in dye-sensitized solar cells, *Nat. Commun.* 7 (2016) 13934.
- [3] N. Gómez-Ortiz, I. Vázquez-Maldonado, A. Pérez-Espadas, G. Mena-Rejón, J. Azamar-Barrios, G. Oskam, Dye-sensitized solar cells with natural dyes extracted from achiote seeds, *Sol. Energy Mater. Sol. Cells* 94 (2010) 40–44.
- [4] W. Ghann, H. Kang, T. Sheikh, S. Yadav, T. Chavez-Gil, F. Nesbitt, J. Uddin, Fabrication, optimization and characterization of natural dye sensitized solar cell, *Sci. Rep.* 7 (2017) 41470.
- [5] S. Kohn, C. Großerhede, J.L. Storck, G. Grötsch, C. Cornelißen, A. Streitenberger, C. Grassmann, A. Schwarz-Pfeiffer, A. Ehrmann, Commercially available teas as possible dyes for dye-sensitized solar cells, *Optik* 185 (2019) 178–182.
- [6] Y. Cao, Y. Saygili, A. Ummadisingu, J. Teuscher, J. Luo, N. Pellet, F. Giordano, S.M. Zakeeruddin, J.-E. Moser, M. Freitag, 11% efficiency solid-state dye-sensitized solar cells with copper (II/I) hole transport materials, *Nat. Commun.* 8 (2017) 15390.
- [7] S. Mathew, A. Yella, P. Gao, R. Humphry-Baker, B.F. Curchod, N. Ashari-Astani, I. Tavernelli, U. Rothlisberger, M.K. Nazeeruddin, M. Grätzel, Dye-sensitized solar cells with 13% efficiency achieved through the molecular engineering of porphyrin sensitizers, *Nat. Chem.* 6 (2014) 242.
- [8] A.B. Marco, N.M. de Baroja, J.M. Andrés-Castán, S. Franco, R. Andreu, B. Villacampa, J. Orduna, J. Garín, Pyranylidene/thienothiophene-based organic sensitizers for dye-sensitized solar cells, *Dye. Pigment.* 161 (2019) 205–213.
- [9] S. Shalini, S. Prasanna, T.K. Mallick, S. Senthilarasu, Review on natural dye sensitized solar cells: operation, materials and methods, *Renew. Sustain. Energy Rev.* 51 (2015) 1306–1325.
- [10] F. Kabir, M. Bhuiyan, M. Hossain, H. Bashar, M. Rahaman, M. Manir, S. Ullah, S. Uddin, M. Mollah, R. Khan, Improvement of efficiency of Dye Sensitized Solar Cells by optimizing the combination ratio of Natural Red and Yellow dyes, *Optik* 179 (2019) 252–258.
- [11] K. Gossen, J.L. Storck, A. Ehrmann, Influence of solvents on Aloe vera gel performance in dye-sensitized solar cells, *Optik* 180 (2019) 615–618.
- [12] Z. Salam, E. Vijayakumar, A. Subramania, N. Sivasankar, S. Mallick, Graphene quantum dots decorated electrospun TiO<sub>2</sub> nanofibers as an effective photoanode for dye sensitized solar cells, *Sol. Energy Mater. Sol. Cells* 143 (2015) 250–259.
- [13] H. Hug, M. Bader, P. Mair, T. Glatzel, Biophotovoltaics: natural pigments in dye-sensitized solar cells, *Appl. Energy* 115 (2014) 216–225.
- [14] G. Calogero, G. Di Marco, S. Cazzanti, S. Caramori, R. Argazzi, A. Di Carlo, C.A. Bignozzi, Efficient dye-sensitized solar cells using red turnip and purple wild sicilian prickly pear fruits, *Int. J. Mol. Sci.* 11 (2010) 254–267.
- [15] G. Calogero, A. Bartolotta, G. Di Marco, A. Di Carlo, F. Bonaccorso, Vegetable-based dye-sensitized solar cells, *Chem. Soc. Rev.* 44 (2015) 3244–3294.
- [16] K. Mukherjee, T.-H. Teng, R. Jose, S. Ramakrishna, Electron transport in electrospun TiO<sub>2</sub> nanofiber dye-sensitized solar cells, *Appl. Phys. Lett.* 95 (2009) 012101.
- [17] S.S. Mali, C.S. Shim, H. Kim, J.V. Patil, D.H. Ahn, P.S. Patil, C.K. Hong, Evaluation of various diameters of titanium oxide nanofibers for efficient dye sensitized solar cells synthesized by electrospinning technique: a systematic study and their application, *Electrochim. Acta* 166 (2015) 356–366.
- [18] M.Y. Song, D.K. Kim, K.J. Ihn, S.M. Jo, D.Y. Kim, Electrospun TiO<sub>2</sub> electrodes for dye-sensitized solar cells, *Nanotechnology* 15 (2004) 1861.
- [19] H. Lund, J. Bjerrum, Eine einfache Methode zur Darstellung wasser-freier Alkohole, *Berichte der deutschen chemischen Gesellschaft (A and B Series)* 64 (1931) 210–213.
- [20] K.J.P. Orton, A.E. Bradfield, CXXXVII.—the purification of acetic acid. The estimation of acetic anhydride in acetic acid, *J. Chem. Soc. (Resumed)* (1927) 983–985.
- [21] H. Zhou, L. Wu, Y. Gao, T. Ma, Dye-sensitized solar cells using 20 natural dyes as sensitizers, *J. Photochem. Photobiol. A: Chem.* 219 (2011) 188–194.
- [22] H. Bashar, M. Bhuiyan, M. Hossain, F. Kabir, M. Rahaman, M. Manir, T. Ikegami, Study on combination of natural red and green dyes to improve the power conversion efficiency of dye sensitized solar cells, *Optik* 185 (2019) 620–625.
- [23] S. Ito, T.N. Murakami, P. Comte, P. Liska, C. Grätzel, M.K. Nazeeruddin, M. Grätzel, Fabrication of thin film dye sensitized solar cells with solar to electric power conversion efficiency over 10%, *Thin Solid Films* 516 (2008) 4613–4619.
- [24] W. Nuansing, S. Ninmuang, W. Jarernboon, S. Maensiri, S. Seraphin, Structural characterization and morphology of electrospun TiO<sub>2</sub> nanofibers, *Mater. Sci. Eng. B* 131 (2006) 147–155.
- [25] D. Li, Y. Xia, Fabrication of titania nanofibers by electrospinning, *Nano Lett.* 3 (2003) 555–560.
- [26] J.-Y. Park, I.-H. Lee, Characterization and morphology of prepared titanium dioxide nanofibers by electrospinning, *J. Nanosci. Nanotechnol.* 10 (2010) 3402–3405.
- [27] S.H. Hwang, C. Kim, H. Song, S. Son, J. Jang, Designed architecture of multiscale porous TiO<sub>2</sub> nanofibers for dye-sensitized solar cells photoanode, *ACS Appl. Mater. Interfaces* 4 (2012) 5287–5292.
- [28] I.C. Maurya, A.K. Gupta, P. Srivastava, L. Bahadur, Callindra haematocephata and Peltophorum pterocarpum flowers as natural sensitizers for TiO<sub>2</sub> thin film based dye-sensitized solar cells, *Opt. Mater.* 60 (2016) 270–276.
- [29] S. Meng, J. Ren, E. Kaxiras, Natural dyes adsorbed on TiO<sub>2</sub> nanowire for photovoltaic applications: enhanced light absorption and ultrafast electron injection, *Nano Lett.* 8 (2008) 3266–3272.
- [30] S. Rajkumar, M.N. Kumar, K. Suguna, S. Muthulakshmi, R.A. Kumar, Enhanced performance of dye-sensitized solar cells using natural cocktail dye as sensitizer, *Optik* 178 (2019) 224–230.
- [31] M. Roy, P. Balraju, M. Kumar, G. Sharma, Dye-sensitized solar cell based on Rose Bengal dye and nanocrystalline TiO<sub>2</sub>, *Sol. Energy Mater. Sol. Cells* 92 (2008) 909–913.
- [32] V.-D. Dao, S.-H. Kim, H.-S. Choi, J.-H. Kim, H.-O. Park, J.-K. Lee, Efficiency enhancement of dye-sensitized solar cell using Pt hollow sphere counter electrode, *J. Phys. Chem. C* 115 (2011) 25529–25534.
- [33] M. Wang, P. Chen, R. Humphry-Baker, S.M. Zakeeruddin, M. Grätzel, The influence of charge transport and recombination on the performance of dye-sensitized solar cells, *ChemPhysChem* 10 (2009) 290–299.